Full Length Research Paper

Automated techniques for quantification of beach change rates using Landsat series along the North-eastern Nile Delta, Egypt

Khalid M. Dewidar[1] and Omran E. Frihy[2]*

[1]Department of Environmental Science, Faculty of Science, Mansoura University, New Damietta City, Box 34517, Egypt.
[2]Coastal Research Institute, 15 El Pharaana Street, 21514, Alexandria, Egypt.

Ten scenes of Landsat sensors (MSS, TM and ETM+) at unequal intervals spanning 35-year period between 1972 and 2007, were analyzed to quantify erosion and accretion pattern along the northeastern coastline of Nile Delta, from Gamasa to Port Said. Rates of shoreline changes were calculated from automated waterline positions generated at 852 locations using a Digital Shoreline Analysis System (DSAS) version 3.2 programs. To assess impacts of coastal structures on the beach morphology the shoreline positions are divided into two groups. The first group (1972 - 1990) is designated to calculate rates of shoreline retreat approximately before protecting the coastline and the second one (1995 - 2007) after construction protection works. Rates of shoreline changes estimated from three statistical approaches of DSAS (the end point rate, the Jackknife and a weighted linear regression) are validated with ground observations of beach profile survey data at the same corresponding positions. Comparison of shoreline rates of beach change obtained from Landsat data with that previously estimated from beach profiles shows that the method used is reasonably accurate with a correlation coefficient value of 0.76. Results indicate that the general alongshore erosion/accretion pattern is locally disrupted by the construction of protective engineering structures. The erosion at the tip of the Damietta promontory is terminated due to the construction of the 6 km seawall built in the year 2000; erosion was originally -43 m/yr before construction of this wall. The 8 km sand spit that has been formed from the eroded zones at the promontory tip before construction of the seawall is now under erosional processes due to deficiency of sediment supply. Further west and prior to protection of Ras El Bar resort, erosion (-10 m/yr) is spatially replaced by a formation of salient accretion (15 m/yr) following emplacement of the detached breakwaters between 1991 and 2002. However, local adverse erosion has been resulted in at the western end of the breakwater system, averaging -5 m/yr. This erosion has resulted from the interruption of the westerly longshore sediment transport by these breakwaters. The seasonal reversal of the NNE waves is responsible for generating of this westward-flowing longshore current along Ras El Bar coastline.

Key words: Shoreline changes, Landsat data, erosion and accession pattern, coastal structures.

INTRODUCTION

The use of Landsat satellite data with facility of spectral, synoptic and near real time data availability has helped in monitoring shoreline changes and monitoring coastal geomorphology (Addo et al., 2008). Now days, coastal zones have been exposed to pressure and processes of change, including urbanization, new infrastructure, exploitation for recreation and tourism. In addition to these infringements are coastal processes such as wind, waves, tide, storm surge, relative sea level rise and land subsidence. Coastline mapping is commonly achieved through the application of different techniques and remote

---

*Corresponding author. E-mail: Frihyomr@yahoo.com. Tel: +203-0103078141.

sensing data varies from fine to moderate spatial resolution. McFeeters (1996) used a Normalized Difference Water Index (NDWI) for detection of water bodies. Waterline can also be mapped through image classification including density slice analysis (Ryan et al., 1991; Gorman et al., 1998; Braud and Feng, 1998; Moore, 2000; Frazier and Page, 2000; Pajak and Leatherman, 2002; Stockdon et al., 2002; Horritt et al., 2003). Time series remotely sensed images with a medium spatial resolution are ideal data sources for mapping coastal land uses and monitoring their changes for a wide area (Shi et al., 2001). Bosworth et al. (2003) used a segmentation technique for multispectral Landsat TM imagery achieved using multiresolution combined with watershed pyramids with region growing approach. Di et al. (2003) investigated a novel approach for automa-tic extraction of shorelines from high-resolution IKONOS satellite imagery using a mean shift segmentation algorithm as a first step and then a local refinement process. Monitoring changes in the coastline is an important task in some applications such as cartography and the environmental management of the entire coastal zone (Dellepiane et al, 2004; Alesheikh et al., 2004). Foody et al. (2005) proposed a technique called a super-resolution mapping approaches applied to the soft classification. Lira (2006) proposed a new methodology to segment open water bodies based on a variant of principal component analysis. The use of satellite remote sensing data was found to be a cost effective approach to quantify the changes over large geographic regions (Sesli et al., 2008). Dewidar and Frihy (2008) used automated waterline technique for detecting pre and post beach response to engineering hard structures in the north-western part of Nile delta from Landsat satellite data.

Similar to other deltas worldwide, the Nile delta is presently subjected to shoreline changes due to a combination of natural and anthropogenic factors. These factors include reduce in Nile delta discharge and sediment loads due to construction of dams and barrages across the Nile River, combined with the action of wave-induced longshore currents (UNDP/UNESCO, 1978). The Aswan High Dam in the Nile River has reduced sediment flux into the sea. Consequently, severe erosion has been resulted in the delta coast (Frihy et al., 2003). This erosion has been mitigated by the construction of a series of coastal engineering structures at the rapidly eroding promontories. These structures include jetties, groins, seawalls and detached breakwaters.

Studies of the shoreline positions and sediment budget along the coast of the Nile delta show that the coastal areas can be divided into a series of discrete sedimentation littoral cells (Frihy et al., 1991). These sub-cells are part of the regional Nile littoral cells extending from Alexandria to Akko on the northern part of Haifa Bay, Israel (Inman and Jenkins, 1984). Each cell contains a coherent trend of littoral transportation and sedimenta-tion, including sources and sinks of sediment and transport paths (Frihy et al., 2003). Sestini (1976), Misdorp (1977) and Frihy (1988) have documented maximum erosion rates of approximately "-"100 m/yr and -10 m/yr at the Rosetta and Damietta promontories, respectively. Analyses of different remote sensing images including Landsat MSS, TM, ETM+ and Spot satellite along parts of the delta have identified areas of erosion followed by beach accretion (Klemas and Abdel Kader, 1982; Smith and Abdel Kader, 1988; Bloget et al., 1991; Frihy et al., 1994; El Raey et al., 1995; White and El Asmar, 1999; Dewidar and Frihy, 2008). The identified pattern has been resulted from wave-induced longshore currents. Higher rates of seabed erosion have been recorded in front of Rosetta and Damietta promontories and Burullus headland (Misdorp and Sestini, 1976; Toma and Salama, 1980). Coastal dynamic processes (Fanos, 1986; El Wany et al., 1988; Nafaa et al., 1991) and sediment transport (Inman and Jenkins, 1984; Frihy et al., 1998; El Sayed et al., 2005; El Banna, 2007) have disclosed the relation between waves induced longshore currents and processes of erosion and accretion along the delta coastline. Texture and mineralogical characteristics of beach sediment versus rates of eroded and accreted parts were discussed by Frihy and Dewidar (1993) and Frihy et al. (1998).

This work is completely different from other studies along the study area. It aims to use automatic techniques to quantify long-term annual rate of beach changes prior to and partially after protection by using series of Landsat image. Also, it includes the effect of protection works on the boundaries and sedimentation pattern of the littoral sub-cells of the northeastern Nile delta.

STUDY AREA

Physical settings

The study coastline spans the northeastern coast of the Nile delta on the Mediterranean coast of Egypt. It extends to about 86 km alongshore from Gamasa drain east of the Burullus headland to the Suez Canal breakwater in Port Said and includes Damietta Nile branch at Ras El Bar resort (Figure 1). The beach sands on the coast of Nile delta are mainly fine to very fine sand (average mean grain size 0.15 mm) but at down drift of coastal areas, they are coarser with mean grain size of about 0.5 mm (Sestini, 1989). These beaches consist of loose quartz sand mixed with small amounts of heavy minerals and shell fragments (Frihy and Dewidar, 2003). The beaches are backed by coastal flats followed by coastal dunes and coastal lagoons in some sectors. Major landuse/ landcover in the study area includes, beach and coastal flats, bare soil, cultivated land, sabakha, salt pan, lagoon, fish farm and urban areas (Figure 1).

Wave data recorded in front of Damietta promontory over 16 months between 1997 and 1999 show wave's direction predo-minant from the N-W sector (81%) with small components from the N-E (14%) and from the S-W (5%) quadrants. The maximum observed wave height is approximately 4.25 m. The averages wave height and period are 0.50 m and 6.5 s, respectively (Frihy et al.,
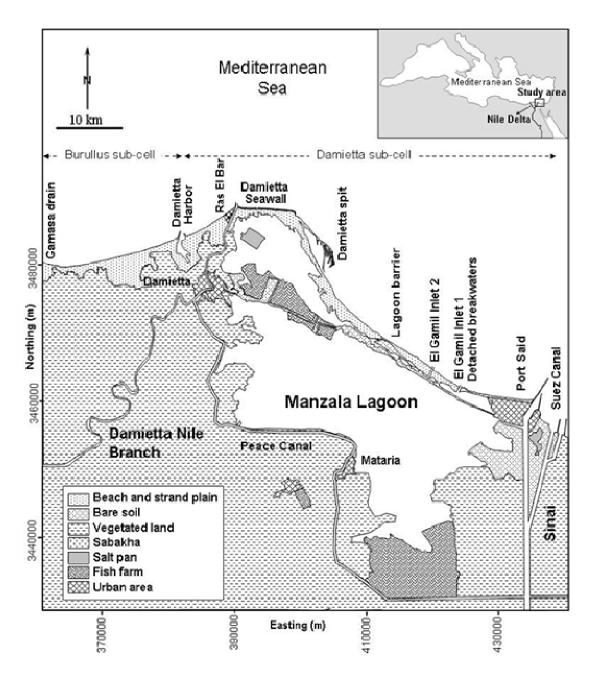
Figure 1. Study area of the Northeastern Nile delta coast, showing major geomorphologic units identified from the Landsat ETM+ 2007 and field observations. Position of Burullus and Damietta sub-cells identified by Frihy et al. (1991) are schematically indicated.

2003). The tide along the delta coast is semi-diurnal with a range 25 – 30 cm. The highest recorded water level is about 80 cm and the lowest level is -64 cm (UNECO/UNDP, 1978).

Protection works

Erosion along the study area has been mitigated by construction of a series of coastal structures including jetties, groins, seawalls and detached breakwaters. In 1941 and 1976, two jetties were constructed on the western and eastern side of Dameitta Nile branch to prevent the deposition of drifted sediment (Figure 2b). To stop severe erosion along south edge of western jetty of Damietta promontory a concrete seawall was constructed in 1963. This seawall has been modified to a rubble seawall to a distance of a bout 1200 m westward of Damietta Nile branch with crest level of ~ 3.5 m above sea level (Fanos et al., 1995; El Banna, 2007). Eight detached breakwaters were constructed between 1991 and 2002 to
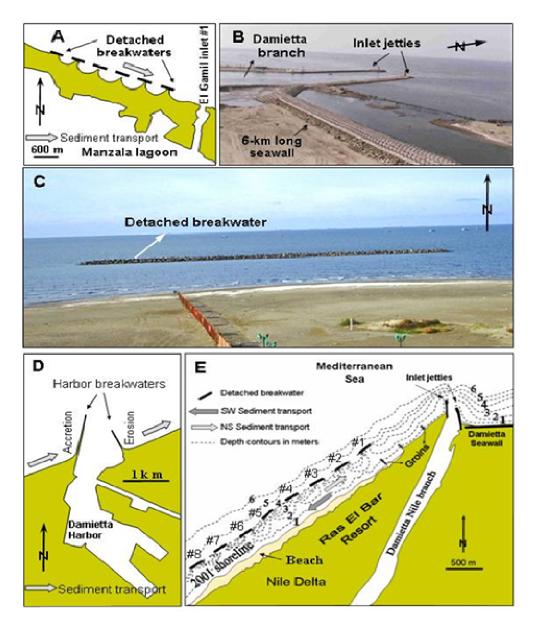
Figure 2. Protection measures constructed at the study area: (A) six detached shore-parallel breakwaters east El Gamil inlet #1, (B) photograph showing the inlet jetties at the Damietta River mouth and the 6 km long seawall built east of the river mouth, (C) photograph of a solitary detached breakwater at Ras El Bar, (D) the Damietta Harbor with its eastern and western breakwaters and (E) eight detached shore-parallel detached breakwaters fronting Ras El Bar resort.

stop erosion along Ras El Bar resort (Figures 2C and E). These detached breakwaters were constructed in 4 m water depth and ~ 400 m from the coastline with 200 m gap width and ~200 m length. Further west, two breakwaters were constructed in 1982 on both sides of Damietta harbor to prevent deposition in the navigation channel (Frihy et al., 2004), Figure 2d. In the year 2000, a 6 km long seawall trending E-W was built onshore along the eastern side of the Nile mouth (Figure 2b), using 4 - 7 ton dolos (concrete blocks). To protect El Gamil Inlet #1 from migration and siltation two jetties were constructed in 1972, 225 and 200 m long, at the wes-

tern and eastern sides, respectively. West of El Gamil Inlet #2, six detached breakwaters were built in 2000 for recreation purpose in the active surfzone at 3 m water depth (Figure 1 for location and Figure 2a). Breakwaters length is 200 m and spaced at 250 m intervals. A small bituminous dike of 3925 m length was constructed to protect the low parts of the coastal road near Port Said from flooding (Fanos et al., 1995). Further east, the northern entrances of the Suez Canal have been stabilized by construction of pairs of long breakwaters in 1870 at each navigation channel (Figure 1). The western entrance channel at Port Said is protected by the

western breakwater that consists of submerged part and emerged one (7.5 km long in total) and eastern breakwater (2.0 km long) (Dewidar and Frihy, 2003). The eastern entrance lay 5 km to the east of the first entrance and is stabilized by the western and eastern breakwaters of 2.0 and 2.25 km long, respectively, (measured in this study from 2007 ETM+ image).

Coastal processes

The study coastline is wave-dominated high-energy environment, in which the principal transporting agents are waves and wave-generated longshore current (Coleman et al., 1981). Wave climate in the form of wave rose is consulted from Frihy et al. (2003). The wave rose (Figure 3a) was generated based on records measured between 1997 and 1999 off the Damietta Harbor using a pressure wave gauge (Inter Ocean System S4DW) installed at ~12 m water depth (Figure 3a, right panel). The average significant wave height and period are 1.04 m and 6.2 s, respectively with a maximum wave height of 4.45 m blown from NW in winter. Wave components exist mainly within two quadrants, the N–W and N–E. The remaining component (10%) represents calm conditions generally with S and SE waves, that is, from inland direction, spanning ~5 % of the time. The N–W waves are of great importance for morpholo-gical processes because of their long duration, particularly in winter and are responsible for generating the net longshore sediment transport to the east along the coast of Nile delta. In contrast, the N–E components occasionally prevail over a short period (~3 – 4 months) and are responsible for generating a reverse long-shore current towards the west, particularly during March and April. Frihy et al. (2003) have indicated that the wave's distribution versus shoreline orientation implies that sand transport is almost eastward unidirectional all year with a significant westward reversal, but with a zero net littoral drift when averaged over several years particularly along the W-E coastal stretches. Reversals of the westward-directed current is significant and occurs if shoreline orientation trending NE-SW such as along Ras El Bar coastline.

MATERIALS AND METHODS

To cross validate rate of beach changes of the eastern coast of the Nile delta, shoreline positions have been determined from both satellite imagery and land survey (beach profiles). A total of 26 profiles (P1 to P26, position in Figure 3a), that cover the study area have been chosen for validation of beach changes estimated before protection of this region (1972 - 1990). These beach profile data are consulted from the study of Frihy and Komar (1993). Beach profile lines are perpendicular to the coastline and extend offshore to about 6 m water depth. The width of the landward part of each beach-profile was measured with an accuracy of ±10 cm. The rate of shoreline change was measured from these sequential beach profiles to a hypothetical baseline applying the least squares technique (Table 1).

In a separate effort, shoreline positions of the study area were extracted from satellite images during a 35 years time span (1972 - 2007). Remote sensing allows the current position of coastlines to be rapidly established at relatively low cost. In addition, future repeated observations over time allow detailed quantification of shoreline change. It has been established that Landsat time series are ideal data sources for mapping coastline and monitoring their changes for wide area (Dewidar and Frihy, 2008). In this study, a series of image data are acquired at unequal intervals between 1972 and 2007, that is, covering a time span of 35 years (Table 2). These series includes ten shorelines: 1972, 1973, 1984, 1990, 1995, 1998, 2000, 2003, 2005 and 2007. The images have been acquired

almost in summer season in good quality, free of clouds or sensor defects such as striping. The study area is encountered in the TM and ETM+ scene (Path/Row 176/38), while it is (Path/Row 190/38 and 191/38) for the MSS. All image scenes are subjected to image processing using ERDAS Imagine software version 8.4 (ERDAS, 1999). In this study, two techniques were used to estimate rate of shoreline retreat. The first technique is corresponding to the formation of automated shoreline positions and the second one is for estimating rate of shoreline change based on a time series of Landsat satellite data applying Digital Shoreline Analysis System (DSAS) software. More details about the processing techniques are cited in the following two sections.

Mapping shoreline position

In this study, automated shoreline positions were formed for each date of image data. The satellite image data were processed according to the following steps:-

Geometric corrections

The study data were geometrically rectified to the Universal Transverse Mercator (UTM) map projection system; zone 36 north, using 35 ground control points evenly distributed within the 2007 Landsat-7 ETM+ scene. The image rectification accuracy is < 0.5 pixel. Other dates of satellite images scenes were registered to the rectified image of date 2007. The image registrations accuracy is < 0.4 pixels between each date and image date 2007.

Atmospheric corrections

In this study, all Landsat image were radiometrically calibrated and converted to reflectance values. The reflectance values of each date were atmospherically corrected by using 6S model (Vermote et al., 1997). Assuming continental type aerosol and with a locally measured visibility value at each date. The atmospheric corrected data was checked with the standard spectral reflectance curve of the materials sand, mud, vegetation and water (Lillesand et al., 2008).

Shoreline position extraction

To extract shoreline position image threshold was formed to band 4 (0.8 - 1.1 µm) for MSS or band 7 (2.0 - 2.35 µm) for TM/ETM+ (shortwave infrared) in each date to form binary image or image mask (zero value for water and one value for land). The selections of these bands depend on the strong capability of water to absorb the incident energy. So the water appears black in color in these bands and sharp edge has been detected between water and land. In order to ensure the waterline mapping accuracy in case of MSS image data 3 x 3 edge enhancement filters was used to sharpen the boundary between water and land classes. Binary images (masked images) were used as input layers in unsupervised classification module to form complete separation between land class and water class and remove effect of suspended materials due to longshore sediment transport. Horizontal and vertical Sobel filters (ERDAS, 1999) were used to each unsupervised classified image of each date to enhance edge detection. Some editing to remove small objects and fill holes is formed for each filtered image in each date. The filtered images for each date were converted to vector layers by using Raster to Vector module (Figure 4). The generated vector maps (Arc Coverage) for the yielded ten shoreline

Table 1. Annual rates of shoreline changes determined from ground survey (Frihy and Komar, 1993) and those estimated from analysis of imagery data (this study). Correlation coefficient values between ground survey and EPR, JKR and WLR, where, EPR = End Point Rate, JKR = Jackknife Rate, WLR = Weighted Line Regression are also indicated. Positive and negative values indicate accretion and erosion respectively. Locations of the examined profiles are shown in Figure 3a.

Profile No.	East (UTM)	North (UTM)	Annual rate of shoreline change (m/yr)			
			From ground Survey	Calculated from DSAS program		
				EPR	JKR	WLR
P1	363743.1	3479671	5.8	1.79	0.38	0.44
P2	364662.2	3479649	3.2	2.59	-0.18	-0.05
P3	366687.4	3479860	2.2	1.79	0.89	0.93
P4	370207.9	3480584	0.9	-3.81	-4.44	-4.41
P5	372571.3	3481104	-1.2	-2.36	-3.73	-3.67
P6	382762.1	3484184	1.2	1.96	-1.24	-1.09
P7	387019.2	3486278	0.3	-0.56	-1.21	-1.18
P8	387937.8	3486786	-0.1	-0.28	-0.23	1.76
P9	388812.6	3487380	-0.2	-5.35	-5.31	-4.32
P10	389493.4	3487997	-0.6	-10.26	-7.2	-6.98
P11	389861.9	3488301	3.2	3.52	2.43	1.89
P12	390255.5	3488801	2.1	0.34	0.48	1.49
P13	390255.5	3488801	0.7	-9.53	-11.71	-12.71
P14	390540.1	3488317	-10.4	-22.64	-19.08	-23.82
P15	394318.9	3488005	-5.1	-36.5	-38.95	-42.55
P16	396760.7	3485497	-4.8	-38.9	-43.84	-42.93
P17	403946.0	3478118	-5.6	-42.1	-44.22	-44.72
P18	396760.7	3485497	1	0.7	-6.51	-6.33
P19	403946.0	3478118	3.5	1.5	0.22	-0.73
P20	407723.5	3473273	-3.3	-5.1	-9.46	-8.44
P21	407723.5	3473273	-6.1	-10.16	-11.36	-12.13
P22	416179.3	3467477	-1.6	-6.23	-9.09	-8.81
P23	420783.8	3464256	13.6	15.14	11.18	13.66
P24	422501.4	3462734	3.7	0.55	0.11	-0.21
P25	426433.3	3461551	-1	-1.36	-1.96	-2.02
P26	431337.3	3460575	1.5	1.48	1.69	1.7
	Correlation coefficient values			0.76	0.72	0.74

Table 2. Acquired dates, sensor type and spatial resolution of landsat sensors data used in this study.

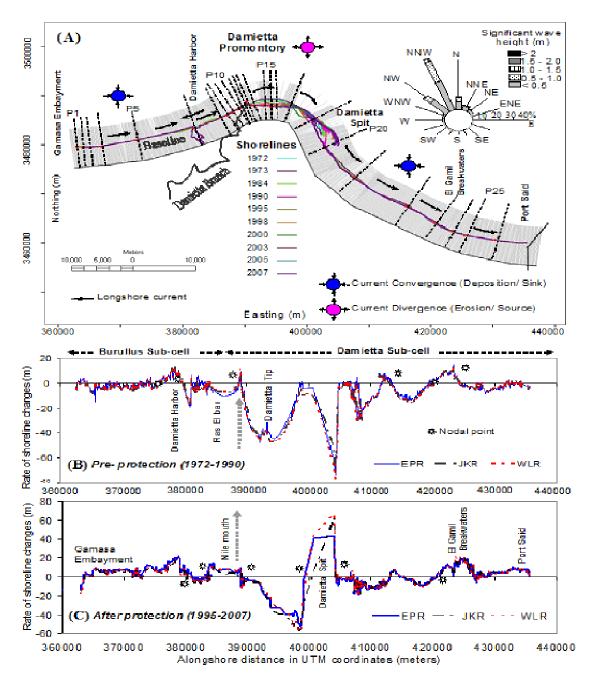| Acquired date	Sensor type	Spatial resolution (meters)
31/08/1972	MSS	57.00
03/01/1973	MSS	57.00
20/09/1984	TM	28.50
04/08/1990	TM	28.50
11/04/1995	TM	28.50
07/06/1998	TM	28.50
11/11/2000	ETM+	14.25
24/08/2003	ETM+	14.25
18/06/2005	ETM+	14.25
04/03/2007	ETM+	14.25

Figure 3. (a) Superimposed shoreline positions alongshore the study area northeastern Nile delta coast extracted from the ten landsat images acquired in 1972, 1973, 1984, 1990, 1995, 1998, 2000, 2003, 2005 and 2007. Solid lines are the 852 cross-shore transects generated to intersect the superimposed vectors and the backshore baseline. Dashed lines (labeled P1 to P26) indicate positions of profiles at which rate of shoreline changes have been calculated from ground survey (Frihy and Komar, 1993). The inset panel shows total deep-water wave rose measured at Damietta Harbor (1997 - 1999), indicating dominant north and northwest frequencies associated with minor northeast reversals (Frihy et al., 2003). Longshore sediment transport direction is schematically diagrammed. (b) Pre- and (c) post- alongshore annual rates of shoreline changes at 852 profiles determined from analysis of imagery data (this study).

positions were processed in geographic information system called ARCGIS software version 9.0 (ESRI, 2004). All shoreline features were then merged within a single line on the attribute table, which enabled the multiple shoreline files to be appended together into a single shapefile (Figure 3a) to calculate the rates of shoreline change with using Digital Shoreline Analysis System (DSAS).
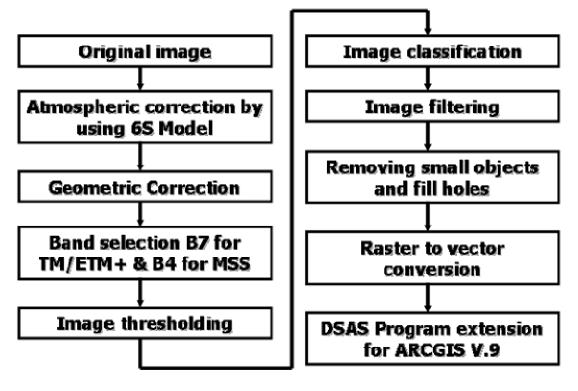
Figure 4. Workflow steps followed in this study to extract image vectors (shoreline positions) and estimating annual rates of beach changes.

Landsat shoreline analysis

In this study a Digital Shoreline Analysis System (DSAS) version 3.2 software developed by Thieler et al. (2005) is used to calculate rate of shoreline changes. This system requires user data to meet specific field requirements. These field requirements includes field name, data type, properties of geographic features. Field widths are generated automatically when a new shapefile or feature class is created. In this study the examined time series of multiple shoreline positions are prepared for these requirements. Based on our setting, DSAS program generates 852 transects that are oriented perpendicular to the baseline at a 100 m spacing alongshore (Figure 3a). These transects span the entire study coastline from Gamasa drain to Suez Canal breakwater (~86 km length). To assess the spatial and temporal migration trend of shoreline positions a hypothetical baseline was created from east to west parallel to the present-day coastline geometry with a position of approximately 4 km distance behind the coastline. The measured distance between the fixed baseline point and the shoreline positions generated by the program provides a reliable record for monitoring the changes of shoreline positions over the 35 years time frame of the generated vectors.

The generated cross-shore transects together with the extracted 10 shoreline vectors are graphically depicted in Figure 3a. The data measured from each profile are then used to estimate the mean annual rate of shoreline change (meter per year) employing linear regression techniques. To assess impacts of coastal structures on the beach morphology the shoreline positions are divided into two groups. The first group (1972 - 1990) is designated to calculate rates of shoreline retreat approximately before protecting the coastline and the second one (1995 - 2007) after construction protection

works. In this study, shoreline retreats were estimated by using three different statistical approaches. The End Point Rate (EPR) is calculated by dividing the distance of shoreline movement by the time elapsed between the earliest and latest measurements at each transect. The Jackknife Rate (JKR) method is implemented as an iterative linear regression that calculates a linear regression fit to shoreline data points with all possible combinations of shoreline points, leaving out one point in each iteration. The Weighted Line Regression (WLR) emphasis on data points where the shoreline position accuracy is lower on certain year (Thieler et al., 2005). The estimate value of Y (dependent variable) is based on a known X (independent variable) in the equation for the regression line ($Y = m X + b$). The standard error of the estimate reflects the degree to which the points diverge from the best fit regression line. In other words, it reflects the accuracy of prediction. The r^2 statistic is the percentage of variance in the data as explained by regression. It is a dimensionless index that ranges from 1.0 to 0.0 and measures how successfully the best fit line accounts for variation in the data. The resulted rates of shoreline changes (erosion or accretion) estimated at each transects are plotted alongshore of the study coastline in Figures 3B and C.

RESULTS AND DISCUSSION

The superimposed annual rates of erosion and accretion calculated from Landsat series using the three different statistical techniques of DSAS (the end point rate, the Jackknife and a weighted linear regression) reveal a good correspondence between them (Figure 3a). To

validate results yielded from the analysis of imagery processing, we consulted rates of shoreline changes calculated from ground survey by Frihy and Komar (1993). A total of 26 profiles (position in Figure 3a) have been chosen for such validation, only spanning the time interval before protection of this region (1972 – 1990). As can be seen in Table 1, results derived from both land survey and satellite imagery at profiles P1 to P26 show good similarity in erosion and accretion pattern but with increase or decrease in rate values in some profiles. Reliability of results is statistically evaluated by correlating rates of shoreline change rates obtained from the two approaches, land survey of Frihy and Komar (1993) and the DSAS (present study) (Table 1). The best fit regression line between rates of shoreline changes calculated from ground survey measurements and those derived from satellite images (DSAS) show reasonably significant correlation coefficient of value 0.76.

As expected, the estimated rates of erosion using the DSAS software along the study area have not been uniform during the examined time intervals, pre- and post protection. Pre- and post alongshore rate of changes show many reversals between erosion and accretion along the length of the study area (Figures 3B and C). This also is accompanied by a considerable variability in shoreline changes in terms of erosion and accretion. This alongshore pattern of shoreline changes and rates of shoreline changes are found to be consistence with the wave refraction orthogonals (wave energy) modeled by Quelennec and Manohar (1977) for waves arriving from the NNW. Results of this model indicate area of convergence orthogonals of high wave energy at the outer margin of the Damietta promontory (source area with current divergence). This area is followed by areas of wave divergence orthogonals of low wave energy along saddle and embayment of this promontory (sink area with current convergence), including Gamasa embayment and central sector of Manzala lagoon barrier.

As can be seen in Figure 3a, a major transport reversal occurs in front of the Damietta promontory, creating a divergent longshore sediment transport to both the west and southeast away from the month. This transport divergence is induced from the effect of high energy waves as indicated by the convergence of the wave orthogonals (Quelennec and Manohar, 1977). Starting from the west, sand derived from continued erosion of the central part of the delta at the Burullus-Baltim beach, ~75 km west of the study site, is transported by the easterly wave-induced littoral current and accumulated within Gamasa embayment. This sub-cell is one of four sub-cells defined along the delta coast by Frihy et al. (1991). The littoral cell in general is defined as a cell contains a complete cycle of littoral transportation and sedimentation, including sources and sinks of sediment and transport paths (Inman and Brush, 1973). The blocking of sediment flow to the east has induced beach erosion (-5 m/yr) east

of the harbor breakwater and accretion on the up-drift side (10 m/yr). On a regional scale, there are many Mediterranean examples of engineering structures that have interfered with sediment transport processes, causing downdrift beach erosion and associated updrift accretion. Significant erosion has been recorded mostly on up-coast (to north) and sand accumulation on updrift side (to south) of most engineering structures constructed along the 197 km Israeli and Gaza strip coastlines, including ports (Gaza, Ashdod, Tel-Aviv, Haifa, Rutenberg), marinas (Ashkelon, Ashdod, Tel-Aviv, Herzliya) , cooling basins (Zikim, Ashdod, Tel-Aviv, Hadera, Haifa, Orot Rabin) detached breakwaters (Ashkelon Dlila, Netanya, Atarim, Hof Hacarmel, Herzliya, Tel-Baruch,) , groins (Al-Agha, 2000; Klein and Zviely, 2001; Rosen, 2002; Klein and Lichter, 2006).

Between 1991 and 2002, a series of eight detached breakwaters were constructed along the coastline of Ras El Bar Resort (Figure 2e). Prior to the construction of these breakwaters, erosion rates between -5.35 m/yr to -10.26 m/yr were estimated in the present study (Figure 3b). These results are closely comparable with those values obtained by White and El Asmar (1999), during the period 1984 to 1990. Following construction of the breakwaters, accretion has become the dominant process with the formation of beach sediments on the leeward side of the structures. This accretion is occurring in a maximum rate of 15 m/yr and has partially filled the shadow area between the coastline and the breakwaters as salient formation. These breakwaters are similar to the detached breakwater system built at Tel Aviv beach, where they lie at somewhat larger distance so that accumulation of tombolos have not been developed (Nir, 1982). As expected, local erosion is observed farther downcoast of these breakwaters at breakwater #8; being approximately 5m/yr (Figure 2e for location). This adverse local erosion has resulted from the interruption of the reversal westward sediment transport by the breakwaters and salient formation, thus increasing sand starvation of downcoast beach. The smaller portion of waves coming from the N and NE is responsible for generation of the reversed longshore currents toward the west at Ras El Bar and thus inducing such local changes (Figure 3c). Results of rate of beach changes obtained in this study are found to be consisted with that calculated from profile data by El Banna and Frihy (2008). The accretionary salient formed in the lee side of these breakwaters has abruptly altered the rate of local erosion in this area before protection. This local erosion averaged 3 m/yr in 1970 - 1990 prior to the building of the breakwaters.

Further east, prior to protection works (1972 - 1990), highest rate of erosion is centered on the Damietta Promontory (-42.1 m/yr) as waves and longshore currents transport sand away from the Damietta headland (Figure 3b). Generally, eroded sand from the tip of Damietta pro-

montory moves toward the east to replenish the downdrift accretionary spit at about 2 km from Damietta river branch. This accretionary coastal feature is typical of wave-dominated deltas and its configuration can be used as an indicator of the net longshore transport direction. Therefore, this spit suggests that it is formed by the easterly movement of sediment, induced by the net longshore current to the east. It was formed approximately between 1955 and 1972 (Frihy and Lawrence, 2004). This spit has been previously discussed by Klemas and Abdel Kader (1982), Frihy (1988) and Smith and Abdel Kader (1988). Similar spits have been formed on the wave dominated Mediterranean delta coastlines.

A high dynamic sand spits have been formed further on both sides of the Ebro river mouth of the Ebro promontory on the coast of Spain (Sanchez-Arcilla et al., 1998). The southern spit has prograded ~700 m, while the northern spit has advanced ~1000 m during 1957 - 1990 period (Jiménez and Sanchez-Arcilla, 1993; Jiménez et al., 1995). In France, a ~3-km long of Gracieuse spit has been formed east of the Rhone delta estuary (Jiménez et al., 1995). In the Po delta of Italy at Goro Po mouth "Scanno di Goro" spit extends seaward for ~5.5 km (Simeoni et al., 1998). This spit was developed in the last 1800 to the early 1900.

In comparison, the estimated massive erosion in the outer margin of the Damietta promontory before protection (-42.1 m/yr) is relatively higher than that measured from beach profile survey (-5.6 m/yr) by Frihy and Komar (1993). This could be attributed to the fact that our analysis is based on a longer term period than that of Frihy and Komar (1993). In contrast, the western flank of the Damietta promontory at Ras El Bar has experienced much less change (-5.35 m/yr to -10.26 m/yr) and this can be attributed to the early protection of this sector in 1941 (Figure 3b). Similar to the Damietta promontory, higher rate of erosion was recorded along the Semani delta promontory of Albania, averaging -78 m/yr, using Landsat images of 1978 - 2001 (Bedini, 2007).

Further east, three nodal points are positioned between Damietta spit and Suez Canal breakwater due to the alternating pattern of erosion and accretion along this area (Figures 3B and C). Nodal points can be positioned at the change or areas of transport from erosion to deposition or vice versa that result from the orientation changes of the shoreline. They can also exist at boundaries of littoral cells that act as a convergent or divergent wave energy (Carter, 1988). Boundaries of littoral cells can also be defined based on the littoral drift patterns of coastal sediments (Cooper and Pontee, 2006). Anfuso et al. (2007) have identified a series of littoral cells terminated by erosion and accretion beach changes along the SW coastline of Spain using longterm marine survey. Beach immediately down coast of the Damietta spit exhibited erosion between -5.1 m/yr and -10.16 m/yr due to sedi-

sediment starvation at the downdrift lee side of this spit (Figure 3c). In contrast the beach accretion (15.14 m/yr) east of El Gamil inlet #2 is caused by the interruption of the prevailing eastward sediment transport by the tombolos formed in the lee side of the constructed six detached breakwaters and thus inducing local morphologic changes (Figures 2a and c).

As the longshore sand transport is almost unidirectional easterly, updrift accretion has taken place at Port Said beach to the west of Suez Canal breakwater (8 m/yr), Figure 3c. Previous studies have confirmed that Port Said beach essentially acts as a sediment sink for sand coming from the erosion of adjacent western shores including Damietta promontory (Frihy and Komar, 1993). The quasi-concave shoreline shape between Damietta spit and Port Said is favorable to trapping longshore transported sediment directed to the east. However, beaches along this sand barrier exhibit local erosion and accession pattern with a maximum value of about 20 m/yr behind El Gamil detached breakwaters. In terms of morphodynamics, the accretion occurs along this sink is produced by the blockage of the eastward longshore sediment transport by the wave breakwater of Port Said. This sink area is a part of the Damietta sub-cell forming a self compartment littoral cell as termed by Frihy et al. (1991) (Figure 1 for location). In this sub-cell, sand eroded from the Damietta promontory is transported to the east where it is trapped naturally by the western breakwater of Suez Canal entrance that results in shoreline accretion. The N-W waves transport sediment is a uniformly east direction along this lagoon sand barrier due to the acute angle of wave attack versus shoreline orientation. Also, there is a transport process accompanied with a westerly seasonal reversals induced from the NNE waves, but the net transport is to the east. We expect that sediment transported to Port Said beach will gradually decease as a result of the extensive engineering structures was built including the 6 km long of the Damietta seawall and the shore-parallel break-water system in El Gamil beach (Figure 2a). Nowadays, the principal source of sediment for Port Said beach is the Damietta spit which start to erosion processes.

Conclusions

Pre- and post- long-term rates of beach changes were determined from the processing of Landsat multi-temporal image data between 1972 and 2007, along the ~86 km length of the northeastern part of the Nile delta. The high rate of beach changes along the study area is now being altered as a response of hard structures built within the littoral cells in particular at Damietta harbor, Ras El Bar and Damietta promontory. As a result, the erosion and accretionary patterns formed along the two littoral cells, namely Burullus and Damietta sub-cells,

have been locally disrupted by these structures. The major protected areas which originally had been acting as a source of sediment for sink areas along promontory saddles and embayment are now diminished. The dramatic erosion centered the tip of the Damietta promontory is terminated due to construction of the 6 km long seawall in the year 2000, originally was -43 m/yr prior to construction. Approximately, 1.5 km cross-shore distance has been lost between 1972 and 2007 as a result of this erosion. Moreover, the chronic erosion along Ras El Bar resort is now replaced by accumulation of a series of continued salient formation (15 m/yr) due to the construction of eight shore parallel detached breakwaters. This former erosion reached up to -5 m/yr prior to protection of this area. As a consequence, the active gyres generated in the gab areas between these breakwaters have caused hazardous effect to swimmers in summer holydays.

Construction of the Damietta harbor has disturbed the shoreline stability causing downdrift erosion and updrift accretion on both sides of the harbor breakwaters. The alongshore variations in the rate of beach changes resulted in a series of nodal points. These nodal points position areas of change from erosion to deposition or vice versa that result from the orientation changes of the shoreline. Although, the geographical boundaries between these sub-cells correspond for the most part to those defined by Frihy et al. (1991), they have been changed following coastal protection works. Therefore, the coastal instability in the study area is mainly due to the combined effects of natural coastal processes (wave-induced current) and construction of protective structures. The present study confirmed the applicability and usefulness of historical Landsat data for change detection analysis of rapidly changes highly energetic coastlines.

REFERENCES

Addo KA, Walkin M, Mills JP (2008). Detection, measurement and prediction of shoreline recession in Accra, Ghana. J. Photogrammetery,Rem.Sens,doi:10.1016/j.isprsjprs.2008.04.001

Al-Agha MR (2000) Access to the coast and erosion control: use of wastes on local engineering works in the coast of Gaza City. Environ. Geol. 39: 405-410.

Alesheikh AA, Ghorbanali A, Talebearer A (2004). Generation the coastline change map for Uremia Lagoon by TM and ETM+ imagery. Map Asia Conference. Beijing, China.

Anfuso G, Martinez JA, Nachite D, Benavente J, Macias A (2007). Morphological characteristics and medium-term evolution of the beaches between Ceuta and Cabo Negro (Morocco). Environ. Geol. 52: 933-946.

Bedini E (2007). Use of GIS and remote sensing to detect change along the coastline segment between Shkumbini and Semani rivers, central Albania. Bulletin of the Geological Society of Greece vol. XXXVII, Proceedings of the 11th International Congress, Athens.

Blodget HW, Taylor PT, Roark JH (1991). Shoreline changes along the Rosetta-Nile Promontory: Monitoring with satellite observations. Mar. Geol. 99: 67-77.

Bosworth J, Koshimizu T, Acton ST (2003). Multi-resolution segmentation of soil moisture imagery by watershed pyramids with region growing merging. Int. J. Rem. Sens. 24: 741-760.

Braud DH, Feng W (1998). Semi-automated construction of the Louisiana coastline digital land/water boundary using Landsat Thematic Mapper satellite imagery. Louisiana Applied Oil Spill Research and Development Program, OSRAPD Technical Report Series 97-002. Department of Geography and Anthropology, Louisiana State University.

Carter RG (1988). Coastal environments. Academic Press, p. 617

Cooper NJ, Pontee NI (2006). Appraisal and evolution of the littoral 'sediment cell' concept in applied coastal management: Experiences from England and Wales. Ocean Coastal Manage. 49: 498–510.

Coleman JM, Robert HH, Murray SP, Salama M (1981) Morphology and dynamic sedimentology of the eastern Nile delta shelf. Mar. Geol. 42: 301- 312.

Dellepiane S, De Laurentiis R, Giordano FG (2004). Coastline extraction from SAR images and a method for the evaluation of coastline precision. Pattern Recognit. Lett. 35: 1461-1470.

Dewidar KH, Frihy OE (2003) Thematic Mapper analysis to identify geomorphologic and sediment texture of El Tineh plain, northwestern coast of Sinai, Egypt. Int. J. Rem. Sens. 24: 2377-2385.

Dewidar KH, Frihy OE (2008). Pre and post-beach response to engineering hard structures using Landsat time-series at the northwestern part of the Nile delta, Egypt. J. Coastal Conserv. 11: 133-142.

DI K, Wang J, MA R, Lı R (2003). Automated shoreline extraction from high resolution IKONOS satellite imagery. In ASPRS 2003 Annual Conference Proceedings, May, Anchorage, Alaska.

EL Asmar HM, White K (2002). Changes in coastal sediment transport processes due to construction of New Damietta Harbor, Nile Delta, Egypt. Coastal Eng. 46: 127–138

EL Banna M (2007). Erosion and accretion rates and their associated sediment characters along Ras El bar coast, northeast Nile Delta, Egypt. Environ. Geol. 52: 41-49.

EL Banna M, Frihy O (2008). Natural and anthropogenic influences in the northeastern coast of the Nile delta, Egypt. Environmental geology, doi: 10.1007/s00254-008-1434-6.

EL Raey M, Nasr SM, EL Hattab MM, Frihy OE (1995). Change detection of Rosetta promontory over the last forty years. Int. J. Rem. Sens. 16: 825-834.

EL Sayed MK, Nazeih AY, Fanos AM, Baghdady KH (2005). Accretion and erosion patterns Rosetta promontory, Nile Delta Coast. J. Coastal Res. 21: 412-420.

EL Wany MH, Khafagy AA, Inman DL, Fanos AM (1988). Analysis of waves from arrays at Abu Quir and Ras El Bar, Egypt, Advanced Underwater Technology Ocean Offshore Eng. 16: 89-97.

ERDAS (1999) ERDAS Field Guide. Atlanta, GA: ERDAS, Inc., p. 698.

ESRI (2004) ARCGIS Desktop version 9. ESRI, 380 New York st., Redlands, USA.

Fanos AM (1986). Statistical analysis of longshore current data along the Nile Delta coast, J. Water Sci. 1: 45-55.

Fanos AM, Khafagy AA, Dean RG (1995). Protective works on the Nile Delta Coast. J. Coastal Res. 11: 516-528.

Foody GM, Muslim AM, Atkinson PM (2005). Super-resolution mapping of the waterline from remotely sensed data. Int. J. Remote Sens. 26: 5381-5392.

Frazier PS, Page KL (2000). Water body detection and delineation with Landsat TM data. Photogrammetric Eng. Rem. Sens. 66: 1467-1467.

Frihy OE (1988). Nile Delta shoreline changes: Aerial photographic study of a 28-year period. J. Coastal Res. 4: 597-606

Frihy OE, Dewidar KH (1993). Influence of shoreline erosion and accretion on texture and heavy mineral compositions of beach sands of the Burullus coast, north central Nile Delta, Egypt. Mar. Geol. 114: 91-104.

Frihy OE, Dewidar Kh (2003). Patterns of erosion/sedimentation, heavy mineral concentration and grain size to interpret boundaries of littoral sub-cells of the Nile Delta. Mar. Geol. 199: 27-43.

Frihy OE, Komar PD (1993). Long-term shoreline changes and the concentrations of heavy minerals in beach sands of the Nile Delta, Egypt. Int. J. Mar. Geol. 115: 253-261.

Frihy OE, Lawrence D (2004). Evolution of the modern Nile delta promontories: development of accretional features during shoreline

retreat. Environmental Geology 46: 914-931.

Frihy OE, Fanos MA, Khafagy AA, Komar PD (1991). Nearshore sediment transport patterns along the Nile Delta Egypt. J. Coastal Eng. 15: 409-429.

Frihy OE, Debes E, EL- Sayed W (2003). Processes reshaping the Nile delta promontories of Egypt: pre and post protection. Geomorphology 53: 263-279.

Frihy OE, Dewidar KH, EL Banna M (1998). Natural and human impact on the northeastern Nile Delta coast of Egypt. J. Coastal Res. 14: 1109-1118.

Frihy OE, EL Banna, MM, EL Kolfat AI (2004). Environmental impacts of Baltim and Ras El Bar shore-parallel breakwater systems on the Nile delta littoral zone, Egypt. Environ. Geol. 45: 381-390.

Frihy OE, Nasr SM, EL Hattab MM, EL Raey M (1994). Remote sensing of beach erosion along the Rosetta promontory, northwestern Nile Delta, Egypt. Int. J. Rem. Sens. 15: 1649-1660.

Gorman L, Morang A, Larson R (1988). Monitoring the coastal environment. IV. Mapping, shoreline changes, and bathymetric analysis. J. Coastal Res. 14: 61-92.

Horritt MS, Mason DC, Cobby DM, Davenport IJ, Bates PD (2003). Waterline mapping in flooded vegetation from airborne SAR imagery. Rem. Sens. Environ. 85: 271-281.

Inman DL, Brush M (1973). The coastal challenge-Fragile ribbons which border our land require more understanding, new technology, and resolute planning. Science 181: 20-32.

Inman DL, Jenkins SA (1984). The Nile littoral cell and man's impact on the coastal zone of the southeastern Mediterranean. Scripps Institution of Oceanography, Reference Series 84-31, University of California, La Jolla, p. 43.

Jiménez JA, Sanchez-Arcilla A (1993). Medium-term coastal response at the Ebro delta, Spain. Mar. Geol. 114: 105-119.

Jiménez J, Capobianco M, Suanez S, Piero,R, Fraunié P, Stive JF (1995). Coastal processes along the Ebro, Po and Rhone deltas, MEDCOAST 95, October 24-27, Tarragona, Spain E. Özhan (Ed), pp.827-840.

Klemas V, Abdel Kader AM (1982). Remote sensing of coastal processes with emphasis on the Nile Delta. International Symposium on Remote Sensing of Environments. (Cairo, Egypt), p. 27

Klein M, Lichter M (2006) Monitoring changes in shoreline position adjacent to the Hadera power station, Israel. Appl. Geogr. 26: 210-226.

Klein M, Zviely D (2001). The environmental impact of marina development on adjacent beaches: a case study of the Herzliya marina, Israel. Appl. Geogr. 21: 145–156

Lira J (2006). Segmentation and morphology of open water bodies from multispectral images. Int. J. Rem. Sens. 27: 4015-4038.

Lillesand TM, Kiefer RW, Chipman JW (2008). Remote Sensing and Image Interpretation. Wiley, Hoboken, NJ.

McFeeters SK (1996). The use of the Normalized Difference Water Index (NDWI) in the delineation of open water features. Int. J. Rem. Sens. 17: 1425-1432.

Misdorp R (1977). The Nile promontories and the Nile continental shelf. In: Proceedings UNESCO Seminar on the Nile Delta coastal Alexandria, pp. 546-551.

Misdorp R, Sestini G (1976) Notes on sediments map of the Endeavour survey of 1919-1922. Proceedings UNESCO Seminar on the Nile Delta Sedimentology, Alexandria, pp. 191-204.

Moore LJ (2000). Shoreline mapping techniques. J. Coastal Res. 16: 11-124.

Nafaa MG, Fanos AM, Khafagy AA (1991) Characteristics of waves off the Mediterranean coast of Egypt. J. Coastal Res. 7: 665-676.

Nir Y (1982). Offshore artificial structures and their influence on the Israel and Sinai Mediterranean beaches. In: Proc 18th International Conference on Coastal Engineering, Cape town, South Africa, pp 1837–1856.

Pajak MJ, Leatherman, S (2002). The high water line as shoreline indicator. J. Coastal Res. 18: 329-337.

Quelennec RE, Manohar M (1977). Numerical wave refraction and computer estimation of littoral drift, application to the Nile Delta coast. Proceedings UNESCO Seminar on Nile Delta Coastal Processes, Academy of Scientific Research and Technology, Alexandria, pp.404-433.

Ryan TW, Sementilli PJ, Yuen P, Hunt BR (1991). Extraction of shoreline features by neural nets and image processing. Photogrammetric Engineering and Remote Sensing 57: 947-955.

Sanchez-Arcilla A, Jiménez JA, Valdemoro HI (1998). The Ebro delta: Morphodynamics and vulnerability. J. Coastal Res. 14:754-772.

Sesli AF, Karsli F, Colkesen I, Akyo IN (2008). Monitoring the changing position of coastlines using aerial and satellite image data: an example from the eastern coast of Trabzon, Turky. Environmental Monitoring and Assessment, DOI 10.1007/s10661 -008-0366-7.

Sestini G (1989). Nile Delta: a review of depositional environments and geological history. Geological Society Special Publication 41:99-127.

Sestini G (1976). Geomorphology of the Nile Delta. CRI/UNDP/
UNESCO, Proceedings Seminar on the Nile Delta Sedimentology (Academic of scientific Research and Technology, Alexandria), pp. 12-24.

Shi Y, Ping D, Shen C (2001). Changes in progradation rate of the tidal flats at the mouth of the Changing (Yangtze) River, China. Geomorphology 38: 167-180.

Simeoni U, Ciavola P, Fontolan G, Mazzini E, Tessari U (1998). Centennial evolution of a re-curved spit: a case study from the spit of the Goro lagoon Po Delta (Italy). Commission International pour l'Exploration Scientifique de la mer Méditerranée (CIESM); In 35th CIESM Congress Proceedings, Dubrovnik (Croatie) 35: 100-101.

Smith ES, Abdel Kader A (1988) Coastal erosion along the Egyptian Delta. J. Coastal Res. 4: 245-255.

Stockdon HF, Sallenger AH, List JH, Holman RA (2002). Estimation of shoreline position and change using airborne topographic Lidar data. J. Coastal Res. 18: 502-513.

Thieler ER, Himmelstoss EA, Zichichi JL, Miller TL (2005). Digital Shoreline Analysis System (DSAS) version 3.0: An ArcGIS extension for calculating shoreline change: U.S. Geological Survey Open-File Report 2005-1304.

Toma SA, Salama MS (1980). Changes in bottom topography of the western shelf of the Nile Delta since 1922. Mar. Geol. 36: 325-3.

Rosen DS (2002). Long-term remedial measures of sedimentological impact due to coastal developments on the south Eastern Mediterranean coast. Littoral, the Changing Coast. EUROCOAST/EUCC, Porto-Portugal. Ed. EUROCOAST-Portugal, pp. 321-331.

UNESCO/UNDP (1978). Coastal protection studies. Final Technical Report, Paris, 1: 155

Vermote FE, Tanre D, Deuze JL, Herman M, Morcrette JJ (1997). Second Simulation of the Satellite Signal in the Solar Spectrum, 6S: An Overview. IEEE Trans. Geosci. Rem. Sens. 35: 675-686.

White K, EL Asmar HM (1999). Monitoring changing position of coastlines using Thematic Mapper imagery, an example from the Nile delta. Geomorphology 29: 93-105.